# H-Atom Abstraction from $CH_3NHNH_2$ by $NO_2$: CCSD(T)/6-311++G(3df,2p)//MPWB1K/6-31+G(d,p) and CCSD(T)/6-311+G(2df,p)//CCSD/6-31+G(d,p) Calculations

**Michael J. McQuaid*,† and Yasuyuki Ishikawa‡**

*U.S. Army Research Laboratory, AMSRD-ARL-WM-BD, Aberdeen Proving Ground, Maryland 21005-5066, and Department of Chemistry, University of Puerto Rico, P.O. Box 23346 San Juan, Puerto Rico 00931-3346*

*Received: January 11, 2006; In Final Form: March 17, 2006*

Stationary points of paths for H atom abstraction from $CH_3NHNH_2$ (monomethylhydrazine) by $NO_2$ were characterized via CCSD(T)/6-311++G(3df,2p)//MPWB1K/6-31+G(d,p) and CCSD(T)/6-311+G(2df,p)//CCSD/6-31+G(d,p) calculations. Five transition states connecting $CH_3NHNH_2-NO_2$ complexes to a manifold that includes $CH_3NHNH-HONO$, $CH_3NNH_2-HONO$, $CH_3NNH_2-HNO_2$, and $CH_3NHNH-HNO_2$ complexes were identified. Transition states that connect $CH_3NHNH-HONO$, $CH_3NNH_2-HONO$, $CH_3NNH_2-HNO_2$, and $CH_3NHNH-HNO_2$ complexes to each other via H atom exchange and/or hindered internal rotation were also identified. The high point in the minimum energy path from the $CH_3NHNH_2 + NO_2$ reactant asymptote to the manifold of HONO-containing product states is a transition state 8.6 kcal/mol above the reactant asymptote. From a kinetics standpoint, this value is considerably higher than the 5.9 kcal/mol value that was estimated for it based on theoretical results for H atom abstraction from $NH_3$ by $NO_2$.

## 1. Introduction

Rocket motors fueled with hypergolic bipropellants—i.e., fuel-oxidizer combinations that ignite spontaneously upon mixing at low temperatures and pressures—are widely employed for propulsion applications requiring active thrust control. Among the most prevalently employed combinations is $CH_3NHNH_2/(NO_2)_2$, which is also referred to as monomethylhydrazine/dinitrogen tetroxide or MMH/NTO.[1] For applications where the freezing point of NTO is too high, MMH/inhibited red fuming nitric acid (IRFNA) is an alternative. IRFNA is mainly nitric acid ($HNO_3$, ~85 wt %) and $NO_2$ (8−15 wt %).

To accelerate the development of hypergolic propulsion systems, computational fluid dynamics (CFD) models are employed to gain insight into the influence of design parameters on engine performance,[2,3] with a chemical kinetics mechanism being among the submodels needed for such efforts. As the starting point for deriving a multistep, finite-rate mechanism that can be used for engines fueled with MMH/NTO or MMH/IRFNA combinations, a "full" chemical-kinetics mechanism is being developed at the US Army Research Laboratory (ARL). The initial version of ARL's mechanism had over 490 distinct reaction steps and involved more than 75 species. Sources for the mechanism include the following: (1) a set of reactions for H/C/N/O compounds that was developed by Anderson and co-workers for modeling the dark zones observed in solid propellant combustion (43 species, 204 reactions),[4] (2) approximately 160 small-hydrocarbon-molecule reactions that were extracted from the GRI 3.0 database,[5] (3) approximately 80 reactions involving $HNO_3$, $NO_3$, $N_2O_4$, and hydrocarbon/$NO_x$ moieties that were identified via a literature search performed specifically for the mechanism development effort, and (4) approximately 50 reactions Catoire and co-workers recommend for modeling the ignition and combustion of $MMH/O_2$ [6] and MMH/NTO [7] systems. The original full mechanism also relied on published estimates for thermochemical parameters of compounds expected to play a role in the combustion of MMH.[8,9]

To check the (original) full chemical kinetics mechanism's validity and completeness, CHEMKIN[10] simulations were run for MMH/NTO systems, and results similar to those reported by Catoire et al.[7] were obtained. In addition, CFD simulations employing a "reduced" chemical kinetics mechanism derived from the full mechanism captured details of rocket-motor-firing combustion chamber pressure vs time results better than simulations employing a more rudimentary treatment of the kinetics.[3] (A reduced chemical kinetics mechanism is utilized because it is impractical to run simulations with the CFD model employing the full chemical kinetics mechanism.) There were, however, several concerns about the full mechanism, and therefore the reduced mechanism, that we felt needed to be addressed.

One concern with the full mechanism is the activation energy specified for the mechanism's representation of the abstraction of an H atom from $CH_3NHNH_2$ by $NO_2$ to form $CH_3NNH_2$ and HONO:

$$CH_3NHNH_2 + NO_2 \rightarrow CH_3NNH_2 + HONO \qquad (1)$$

H atom abstraction has long been postulated to be a rate-controlling step in the initiation of hydrazine/NTO and hydrazine-derivative/NTO systems.[11,12] Moreover, though IRFNA is primarily composed of nitric acid, there is evidence that IRFNA's NTO fraction plays a critical role in the ignition of IRFNA-oxidized systems.[13] The importance of reaction 1 during the pre-ignition phase of the propulsion cycle is also suggested by CHEMKIN simulations based on the full MMH/IRFNA chemical kinetics mechanism. Performed for MMH/NTO and MMH/IRFNA mixtures, sensitivity analyses conducted in conjunction with the simulations identify its importance, and a significant lengthening of the time between reaction/simulation start and the onset of ignition-like behavior was observed when the activation energy employed in the Arrhenius description of reaction 1's rate was increased.

* Corresponding author: E-mail: mcquaid@arl.army.mil Fax: (410) 306-1909.
† U.S. Army Research Laboratory, AMSRD-ARL-WM-BD.
‡ University of Puerto Rico.

10.1021/jp060210j CCC: $33.50 
Published on Web 04/19/2006

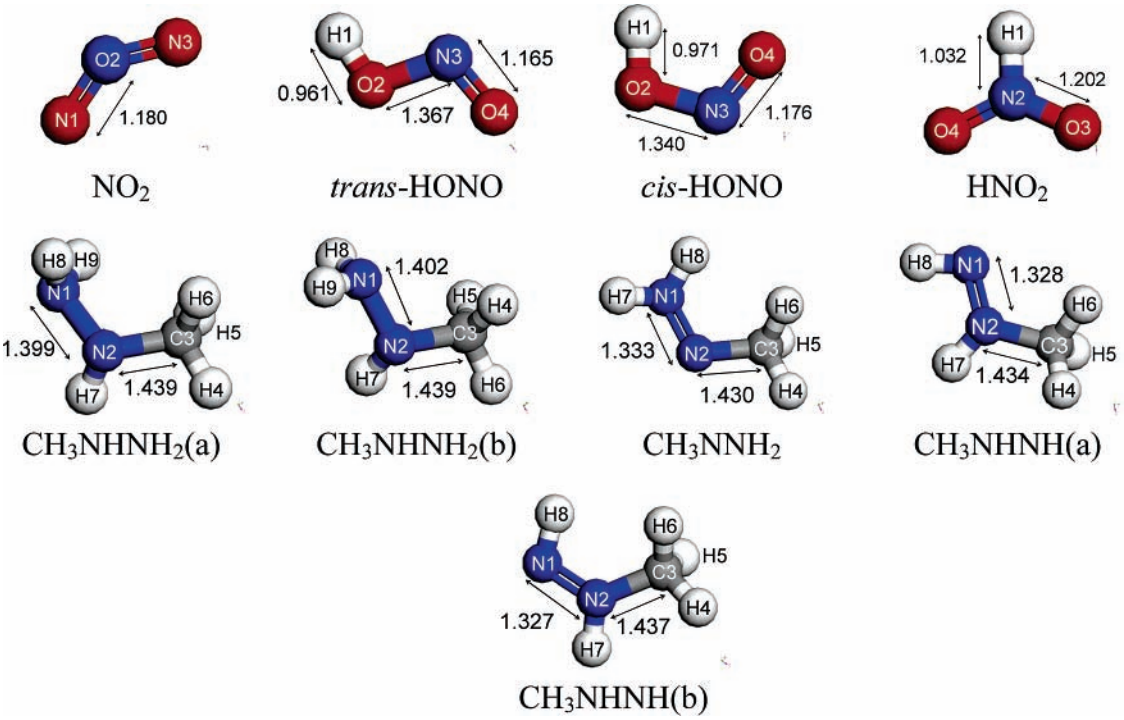


**Figure 1.** Reactants and products for the $CH_3NHNH_2 + NO_2$ system. The bond lengths shown (in angstroms) are from MPWB1K/6-31+G(d,p) optimizations.

Our concern about the activation energy employed for reaction 1 in the chemical kinetics mechanism stems from the fact that it is estimated using theoretical results for analogous $NH_3 + NO_2$ H atom abstraction reactions.[14] Considering that approach to have limited merit,[9] we have been seeking to characterize the energetics of $CH_3NHNH_2 + NO_2$ H atom abstraction paths directly. But the task proved difficult, and there was reason to believe that none of the previously found paths corresponded to the minimum energy path for the reaction. Thus, their relevance to the kinetics of MMH/NTO and MMH/IRFNA systems was considered suspect.[9] The study reported here addresses the concerns that were raised.

Another issue of concern has been the fact that reaction 1 is the only equation included in the full chemical kinetics mechanism for the reaction of MMH with $NO_2$. As such, it belies the complexity of the system observed and described at a molecular level. For example, it neglects the fact that HONO has cis and trans isomers. To include them as distinct species in the mechanism would require that

$$CH_3NHNH_2 + NO_2 \rightarrow CH_3NNH_2 + \textit{trans}\text{-HONO} \quad (2)$$

and

$$CH_3NHNH_2 + NO_2 \rightarrow CH_3NNH_2 + \textit{cis}\text{-HONO} \quad (3)$$

be specified in lieu of reaction 1. H atom abstraction reactions with the potential to produce $HNO_2$

$$CH_3NHNH_2 + NO_2 \rightarrow CH_3NNH_2 + HNO_2 \quad (4)$$

and $CH_3NHNH$

$$CH_3NHNH_2 + NO_2 \rightarrow CH_3NHNH + \textit{trans}\text{-HONO} \quad (5)$$

$$CH_3NHNH_2 + NO_2 \rightarrow CH_3NHNH + \textit{cis}\text{-HONO} \quad (6)$$

$$CH_3NHNH_2 + NO_2 \rightarrow CH_3NHNH + HNO_2 \quad (7)$$

are not included in the mechanism either.

We also considered the need to include H atom abstraction from $CH_3NHNH_2$'s methyl group:

$$CH_3NHNH_2 + NO_2 \rightarrow CH_2NHNH_2 + \textit{trans}\text{-HONO} \quad (8)$$

$$CH_3NHNH_2 + NO_2 \rightarrow CH_2NHNH_2 + \textit{cis}\text{-HONO} \quad (9)$$

$$CH_3NHNH_2 + NO_2 \rightarrow CH_2NHNH_2 + HNO_2 \quad (10)$$

However, we verified our expectation (based on the dissociation energies typical of C−H and N−H bonds) that the endothermicities of these reactions will be significantly more positive than their reaction 2−7 counterparts. [On the basis of the CCSD(T)/6-311++G(3df,2p)//MPWB1K/6-31+G(d,p)[15−24] model discussed below, they are approximately 15 kcal/mol more endothermic.] So we assume that such reactions will have little (if any) impact on the dynamics of MMH/NTO and MMH/IRFNA systems, particularly at the low temperatures (300−600 K) in a rocket motor combustion chamber prior to ignition. We likewise assume that $NO_2$ will not prompt MMH's C−N or N−N bonds to break.

Similarly, $HNO_2$ is 8.1 kcal/mol higher in energy than *trans*-HONO. Thus, the omission of reactions 4 and 7 seems warranted. However, the case for representing reactions 2 and 3 with one equation is less clear. Though the difference in energy between the cis and trans isomers of HONO is only about 0.3 kcal/mol, in the case of $NH_3 + NO_2$ H atom abstraction reactions, the difference in energy between the barriers to their formation has been calculated to be approximately 11 kcal/mol.[14] In addition, we find the barrier to *cis*-HONO ↔ *trans*-HONO isomerization (via unimolecular hindered internal rotation) to be approximately 10.7 kcal/mol. Such differences/barriers are nontrivial at 300−600 K. And since the activation energies for their formation are different, it can be imagined that their subsequent decomposition paths are different as well.

Justification for neglecting $CH_3NHNH$ production is also lacking. Like HONO, $CH_3NHNH$ has (at least) two low-energy conformers, the difference in their energies are small (0.2 kcal/

**TABLE 1: MMH + $NO_2$ H Atom Abstraction Reactions: Reactant and Product Zero-Point Corrected Energies**

| | ZPVE[a] (kcal/mol) | method A[b] (hartrees) | Δ[c] (kcal/mol) | method B[d] (hartrees) | Δ[e] (kcal/mol) |
|---|---|---|---|---|---|
| $NO_2$ | 5.7 | −204.781647 | 0.0 | −204.792928 | 0.0 |
| *trans*-HONO | 13.0 | −205.399807 | 0.0 | −205.412534 | 0.0 |
| *cis*-HONO | 12.9 | | 0.4 | | 0.3 |
| $HNO_2$ | 13.9 | | 8.0 | | 8.1 |
| HONO(TS)[f] | 11.6 | | | | 10.7 |
| $CH_3NHNH_2$(a) | 50.4 | −150.827974 | 0.0 | −150.845690 | 0.0 |
| $CH_3NHNH_2$(b) | 50.4 | | 0.7 | | 0.7 |
| $CH_3NHNH_2$(TS1)[g] | 50.1 | | | | 2.7 |
| $CH_3NHNH_2$(TS2)[g] | 49.8 | | | | 8.0 |
| $CH_3NNH_2$ | 41.7 | −150.209549 | 0.0 | −150.225306 | 0.0 |
| $CH_3NHNH$(a) | 42.0 | | 2.4 | | 2.1 |
| $CH_3NHNH$(b) | 42.0 | | 2.6 | | 2.3 |
| $CH_3NHNH$(TS)[h] | 40.5 | | | | 23.1 |
| $CH_2NHNH_2$ | 41.9 | | | | 14.2 |

[a] Scaled MPWB1K/6-31+G(d,p) result. [b] CCSD(T)/6-311+G(2df,p)//CCSD/6-31+G(d,p) [c] Difference in CCSD(T)/6-311+G(2df,p)//CCSD/6-31+G(d,p) energy relative to lowest energy, stoichiometrically equivalent molecule. [d] CCSD(T)/6-311++G(3df,2p)//MPWB1K/6-31+G(d,p) [e] Difference in CCSD(T)/6-311++G(3df,2p)//MPWB1K/6-31+G(d,p)) energy relative to lowest energy, stoichiometrically equivalent molecule. [f] *trans*-HONO ↔ *cis*-HONO transition state. [g] $CH_3NHNH$(a) ↔ $CH_3NHNH_2$(b) transition state. [h] $CH_3NHNH$(a) ↔ $CH_3NHNH$(b) transition state.

**TABLE 2: Reactant and Product Geometric Parameters: Comparison of MPWB1K/6-31+G(d,p) and CCSD/6-31+G(d,p) Results[a]**

| | MPWB1K | CCSD | Δ | | MPWB1K | CCSD | Δ |
|---|---|---|---|---|---|---|---|
| $NO_2$ | | | | $CH_3NHNH_2$(b) | | | |
| N2−O1/N2−O3 | 1.180 | 1.204 | −0.024 | N2−N1 | 1.402 | 1.435 | −0.033 |
| O3−N2−O2 | 134.8 | 134.4 | 0.5 | C3−N2 | 1.439 | 1.461 | −0.021 |
| | | | | H7−N2 | 1.009 | 1.017 | −0.008 |
| *trans*-HONO | | | | H8−N1 | 1.011 | 1.018 | −0.008 |
| O2−H1 | 0.961 | 0.970 | −0.009 | H9−N1 | 1.005 | 1.013 | −0.008 |
| N3−O2 | 1.367 | 1.417 | −0.050 | C3−N2−N1 | 110.8 | 109.5 | 1.3 |
| O4−N3 | 1.165 | 1.185 | −0.020 | H7−N2−C3−H5 | 65.8 | 63.8 | 2.0 |
| N3−O2−H1 | 104.2 | 103.0 | 1.2 | H8−N1−N2−H7 | −38.4 | −34.8 | −3.6 |
| O4−N3−O2 | 111.2 | 110.5 | 0.7 | H9−N1−N2−H7 | 83.9 | 84.2 | −0.3 |
| O4−N3−O2−H1 | 180.0 | −180.0 | 0.0 | | | | |
| | | | | $CH_3NNH_2$ | | | |
| *cis*-HONO | | | | N2−N1 | 1.333 | 1.363 | −0.030 |
| O2−H1 | 0.971 | 0.979 | −0.007 | C3−N2 | 1.430 | 1.454 | −0.024 |
| N3−O2 | 1.340 | 1.388 | −0.047 | H7−N2 | 1.003 | 1.009 | −0.007 |
| O4−N3 | 1.176 | 1.196 | −0.020 | H8−N1 | 1.011 | 1.018 | −0.007 |
| N3−O2−H1 | 106.9 | 105.8 | 1.1 | C3−N2−N1 | 110.2 | 109.3 | 0.9 |
| O4−N3−O2 | 113.4 | 113.1 | 0.4 | H7−N2−C3−H5 | −168.2 | −166.1 | −2.2 |
| O4−N3−O2−H1 | 0.0 | 0.0 | 0.0 | H8−N1−N2−H7 | −28.9 | −33.5 | 4.5 |
| $HNO_2$ | | | | $CH_3NHNH$(a) | | | |
| N2−H1 | 1.032 | 1.034 | −0.002 | N2−N1 | 1.328 | 1.355 | −0.028 |
| O3−N2/O4−N2 | 1.202 | 1.226 | −0.024 | C3−N2 | 1.434 | 1.454 | −0.020 |
| O3(4)-N2−H1 | 115.9 | 115.9 | 0.0 | H7−N2 | 1.007 | 1.014 | −0.007 |
| O4−N3−O2 | 128.2 | 128.1 | 0.1 | H8−N1 | 1.015 | 1.024 | −0.009 |
| O4−N2−O3−H1 | 180.0 | 180.0 | 0.0 | C3−N2−N1 | 116.5 | 115.2 | 1.3 |
| | | | | H7−N2−C3−H5 | 77.6 | 72.8 | 4.8 |
| $CH_3NHNH_2$(a) | | | | H8−N1−N2−H7 | 22.0 | 26.4 | −4.4 |
| N2−N1 | 1.399 | 1.431 | −0.032 | | | | |
| C3−N2 | 1.439 | 1.461 | −0.022 | $CH_3NHNH$(b) | | | |
| H7−N2 | 1.005 | 1.013 | −0.008 | N2−N1 | 1.327 | 1.354 | −0.028 |
| H8−N1 | 1.006 | 1.013 | −0.007 | C3−N2 | 1.437 | 1.458 | −0.021 |
| H9−N1 | 1.013 | 1.020 | −0.007 | H7−N2 | 1.003 | 1.010 | −0.007 |
| C3−N2−N1 | 114.6 | 113.7 | 0.9 | H8−N1 | 1.017 | 1.025 | −0.008 |
| H7−N2−C3−H5 | 69.4 | 65.8 | 3.5 | C3−N2−N1 | 122.7 | 121.1 | 1.7 |
| H8−N1−N2−H7 | 148.3 | 151.4 | −3.1 | H7−N2−C3−H5 | 81.3 | 75.6 | 5.7 |
| H9−N1−N2−H7 | −91.4 | −90.7 | −0.7 | H8−N1−N2−H7 | −171.0 | −169.0 | −1.9 |

[a] Bond lengths in angstroms, simple angles and dihedral angles in degrees.

mol), and the barrier to hindered internal rotation that separates them is relatively large (21.0 kcal/mol). Moreover, unlike the 8.1 kcal/mol difference between *trans*-HONO and $HNO_2$, the $CH_3NHNH$ conformers are only about 2 kcal/mol higher in energy than $CH_3NNH_2$. Coupled with the fact that abstraction of an H atom from $CH_3NNH_2$ is expected to form only $CH_3NNH$ while the abstraction of an H atom from $CH_3NHNH$ could produce $CH_3NHN$ as well, if $CH_3NHNH$ ↔ $CH_3NNH_2$ isomerization is not facile, then the omission of reactions 5 and 6 might not be justified. This matter is considered in this paper.

## 2. Computational Methods

Mechanisms for the abstraction of an H atom from $CH_3NHNH_2$ by $NO_2$ were searched for and stationary point structures characterized via MPWB1K/6-31+G(d,p)[15−18] geometry optimizations. MPWB1K is a hybrid meta density

**TABLE 3: ZPVEs and Relative Zero-Point Corrected Energies of Local Minima and Transition States Associated with MMH + $NO_2$ H Atom Abstraction Reactions (kcal/mol)**

| | type | ZPVE[a] | RE[b] | RE[c] |
|---|---|---|---|---|
| A | min | 57.0 | −1.7 | −2.7 |
| B | TS | 54.3 | 11.6 | 12.2 |
| C | min | 56.9 | −2.6 | −3.5 |
| D | TS | 54.4 | 4.8 | 3.7 |
| E | min | 56.4 | −8.5 | −9.0 |
| F | min | 56.9 | −3.1 | −2.7 |
| G | TS | 55.5 | 9.6 | 10.3 |
| H | min | 57.0 | −2.2 | −2.3 |
| I | TS | 53.9 | 4.8 | 3.8 |
| J | min | 56.1 | −10.4 | −10.7 |
| K | min | 57.3 | −3.2 | −3.1 |
| L | TS | 55.9 | 10.4 | 10.1 |
| M | min | 55.9 | −8.8 | −8.8 |
| N | min | 57.3 | −0.6 | 0.2 |
| O | TS | 55.5 | 10.6 | 9.5 |
| P | min | 56.0 | −6.4 | −6.6 |
| Q | min | 57.2 | −0.8 | −0.5 |
| R | TS | 55.7 | 11.2 | 8.6 |
| S | min | 56.1 | −8.9 | −9.2 |
| T | TS | 55.3 | | 7.8 |
| U | min | 56.1 | | −6.2 |
| V | TS | 55.9 | | −5.9 |
| W | TS | 54.6 | | −4.4 |
| X | min | 55.9 | | −10.7 |
| Y | TS | 54.9 | | 2.5 |
| Z | TS | 54.8 | | 0.9 |

[a] Scaled MPWB1K/6-31+G(d,p) result. [b] Energy relative to MMH(a) + $NO_2$ reactant asymptote: CCSD(T)/6-311++G(2df,p)//CCSD/6-31+G(d,p) result. [c] Energy relative to MMH(a) + $NO_2$ reactant asymptote: CCSD(T)/6-311++G(3df,2p)//MPWB1K/6-31+G(d,p) result.

functional theory (DFT) method developed by Truhlar et al.,[15] who demonstrated its efficacy for predicting thermochemical properties, H-bonding, van der Waals interactions, and transition state geometries for a range of structures and reactions, most of the transition states being associated with H atom abstractions.

Our decision to utilize MPWB1K for the study was made after trying more commonly employed methods. The methods tried included B3LYP/6-311++G(d,p),[18,25−28] MPW1K/6-31+G(d,p),[16−18,29] MP2/6-311++G(d,p)[18,28,30−34] and CCSD/6-31+G(d,p),[16−18,19−22] with conclusions about their utility being drawn from the search for transition states for $NH_2NH_2$ + $NO_2$ H atom abstraction reactions as well as the subject reactions. Briefly, the success achieved with them was deemed limited.[9] In particular, transition states directly connecting $CH_3NHNH_2$−$NO_2$ complexes with $CH_3NNH_2$−*cis*-HONO or $CH_3NHNH$−*cis*-HONO complexes could not be found, and, on the basis of Mebel et al.'s results for $NH_3$ + $NO_2$, such transition states were expected to have lower energies than the transition states that had been found.

A combination of numerical instability (related to spin contamination), computational demands, and the propensity of geometry optimizations to walk toward "H atom exchange" transition states led to the failure of most ab initio model [MP2/6-311++G(d,p) and CCSD/6-31+G(d,p)] transition state geometry optimizations that did not start close to a converged solution. (H atom exchange transition states are those connecting one $CH_3NNH_2$−HONO or $CH_3NHNH$−HONO complex with another.) Beyond failing to find some transition states that were expected on the basis of Mebel et al.'s results, the DFT models [B3LYP/6-311++G(d,p) and MPW1K/6-31+G(d,p)] identified several structures as transition states, but their existence/nature could not be corroborated via subsequent CCSD/6-31+G(d,p) calculations. Their mappings of the potential energy surfaces of the hydrazine + $NO_2$ and MMH + $NO_2$ systems were therefore considered suspect and led us to search for an alternative.

MPWB1K/6-31+G(d,p) was found to produce results for MMH + $NO_2$ reaction paths that were similar to ones previously established via CCSD/6-31+G(d,p) calculations. In addition, optimizations with the model were able to find other transition state structures whose existence was expected on the basis of Mebel et al.'s results.[14] MPWB1K/6-31+G(d,p) intrinsic reaction coordinate (IRC) trajectory calculations[35,36] were employed to confirm the identity of the connecting intermediate (local minimum) states. Moreover, once found via an MPWB1K/6-31+G(d,p) optimization, newly identified transition states were quickly found via subsequent CCSD/6-31+G(d,p) optimizations. Issues related to spin contamination were also addressed. For all open-shell, MPWB1K/6-31+G(d,p)-optimized structures, the reference state $\langle S^2 \rangle$ values were between 0.755 and 0.761, and their DFT $\langle S^2 \rangle$ values (after annihilation) were within 0.0001 of their actual value (0.7500). Reference state $\langle S^2 \rangle$ values as high as 1.043 were observed for open-shell, CCSD/6-31+G(d,p)-optimized structures. However, in all cases, $\langle S^2 \rangle$ values for their correlated wave functions were within 0.011 of their actual value.

The results reported here were obtained with the Gaussian 03 (G03) suite of quantum chemistry codes.[37] The convergence criteria specified for the geometry optimizations were maximum force $\leq$ 0.000450 hartree/bohr, root-mean-square (RMS) force $\leq$ 0.00300 hartree/bohr, maximum displacement $\leq$ 0.001800 bohr, and RMS displacement $\leq$ 0.001200 bohr. Normal-mode analyses of the MPWB1K/6-31+G(d,p) structures were performed to confirm that geometries meeting the convergence criteria were indeed local minima or transition states. To establish zero-point corrected energies (ZPE) for reaction-path stationary points, the electronic energies of MPWB1K/6-31+G(d,p) optimized structures were computed with a CCSD(T)/6-311++G(3df,2p) model and (scaled) zero-point vibrational energies (ZPVEs) determined in conjunction with the MPWB1K/6-31+G(d,p) frequency calculations were added to them. The scaling factor employed to adjust the ZPVEs was 0.957.[15] All of the relative energies referred to in the text are zero-point corrected values unless otherwise noted.

CCSD(T)/6-311+G(2df,p)//CCSD/6-31+G(d,p) results were also obtained for many of the stationary points found with MPWB1K/6-31+G(d,p). In a previously reported study,[9] relative energies for a subset of the CCSD/6-31+G(d,p) structures reported here were obtained with a "G2I" protocol. However, some anomalous results were observed. They are now recognized to be associated with the influence of spin contamination in MP2 results that were employed to correct the CCSD(T)/6-311+G(2df,p)//CCSD/6-31+G(d,p) results for basis set truncation errors. Therefore, this "correction" is omitted here. The current approach also leaves out the semiempirical "higher level correction." From the standpoint of characterizing MMH + $NO_2$ reaction paths, its inclusion is unnecessary because it is the same for all of the stationary points considered.

Another difference between the CCSD(T)/6-311+G(2df,p)//CCSD/6-31+G(d,p) results reported here and the G2I//CCSD/6-31+G(d,p) results reported previously is in the basis for the ZPVE corrections. In the G2I protocol, unscaled ZPVEs from CCSD/6-31+G(d,p) frequency calculations were employed. However, the computational resources required to obtain those corrections were difficult to justify. Therefore, only ZPVEs for transition states were obtained; in their case, the need for

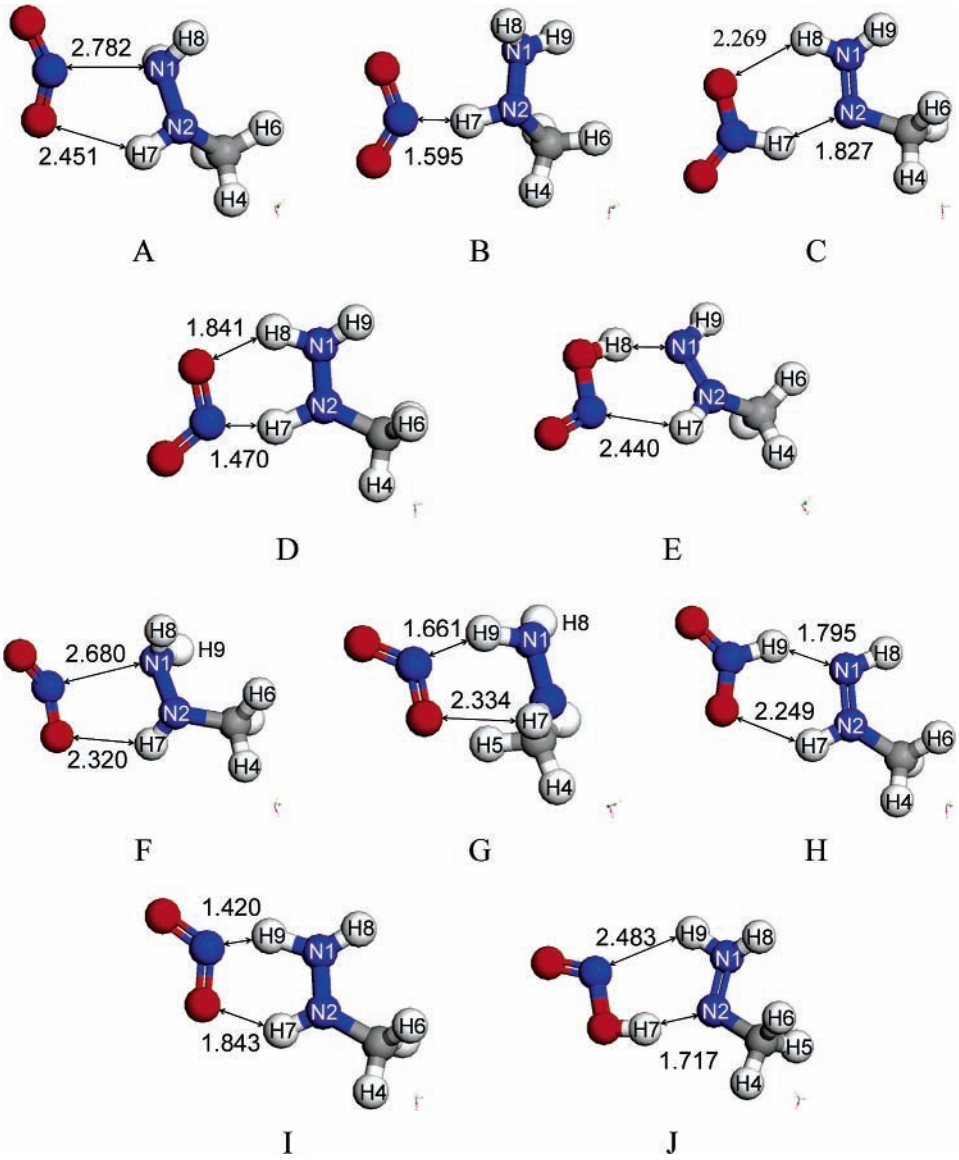


**Figure 2.** Local minima and transition states for the $CH_3NHNH_2 + NO_2$ potential energy surface: configurations A−J. Bond lengths are in angstroms.

**TABLE 4: Comparison of Selected Bond Lengths (Angstroms) for Transition State Structures: MPWB1K/6-31+G(d,p) vs CCSD/6-31+G(d,p) Results**[a]

| bond/structure | $NO_2$ | *t*-HONO | *c*-HONO | MMH | B | D | G | I | L | O | R |
|---|---|---|---|---|---|---|---|---|---|---|---|
| N2−H7 | | | | 1.005 | 1.072 | 1.141 | 1.006 | 1.028 | 1.006 | 1.010 | 1.005 |
| | | | | (1.013) | (1.090) | (1.162) | (1.012) | (1.028) | (1.012) | (1.017) | (1.012) |
| N1−H8 | | | | 1.006 | 1.005 | 1.006 | 1.009 | 1.007 | 1.011 | 1.036 | 1.007 |
| | | | | (1.013) | (1.012) | (1.026) | (1.017) | (1.013) | (1.018) | (1.054) | (1.015) |
| N1−H9 | | | | 1.013 | 1.005 | 1.028 | 1.066 | 1.168 | 1.010 | 1.005 | 1.040 |
| | | | | (1.020) | (1.013) | (1.012) | (1.078) | (1.183) | (1.017) | (1.014) | (1.057) |
| $N_{NO2}-H_{abs}$ | | | | | 1.595 | 1.470 | 1.661 | 1.420 | | | |
| | | | | | (1.546) | (1.437) | (1.629) | (1.402) | | | |
| $H_{abs}$-O(−N) | | 0.961 | 0.971 | | 3.713 | 1.841 | 2.334 | 1.843 | 2.170 | 1.829 | 1.774 |
| | | (0.970) | (0.979) | | (3.563) | (1.956) | (2.460) | (1.926) | (2.246) | (1.717) | (1.685) |
| (H−)O−N | 1.180 | 1.367 | 1.340 | | 1.203 | 1.248 | 1.217 | 1.247 | 1.224 | 1.213 | 1.216 |
| | (1.204) | (1.417) | (1.388) | | (1.222) | (1.270) | (1.231) | (1.271) | (1.245) | (1.248) | (1.250) |
| (O−)N−O | 1.180 | 1.165 | 1.176 | | 1.205 | 1.206 | 1.200 | 1.205 | 1.231 | 1.203 | 1.203 |
| | (1.204) | (1.185) | (1.196) | | (1.225) | (1.227) | (1.217) | (1.226) | (1.273) | (1.225) | (1.223) |

[a] CCSD/6-31+G(d,p) results are in parentheses.

frequency calculations to confirm that they were indeed saddle points being compelling. For this study, ZPVEs for all relevant structures were desired. Therefore, scaled ZPVEs from MPWB1K/6-31+G(d,p) frequency calculations were employed to obtain zero-point corrected CCSD(T)/6-311+G(2df,p)//CCSD/6-31+G(d,p) results. For the five transition states for which both CCSD/

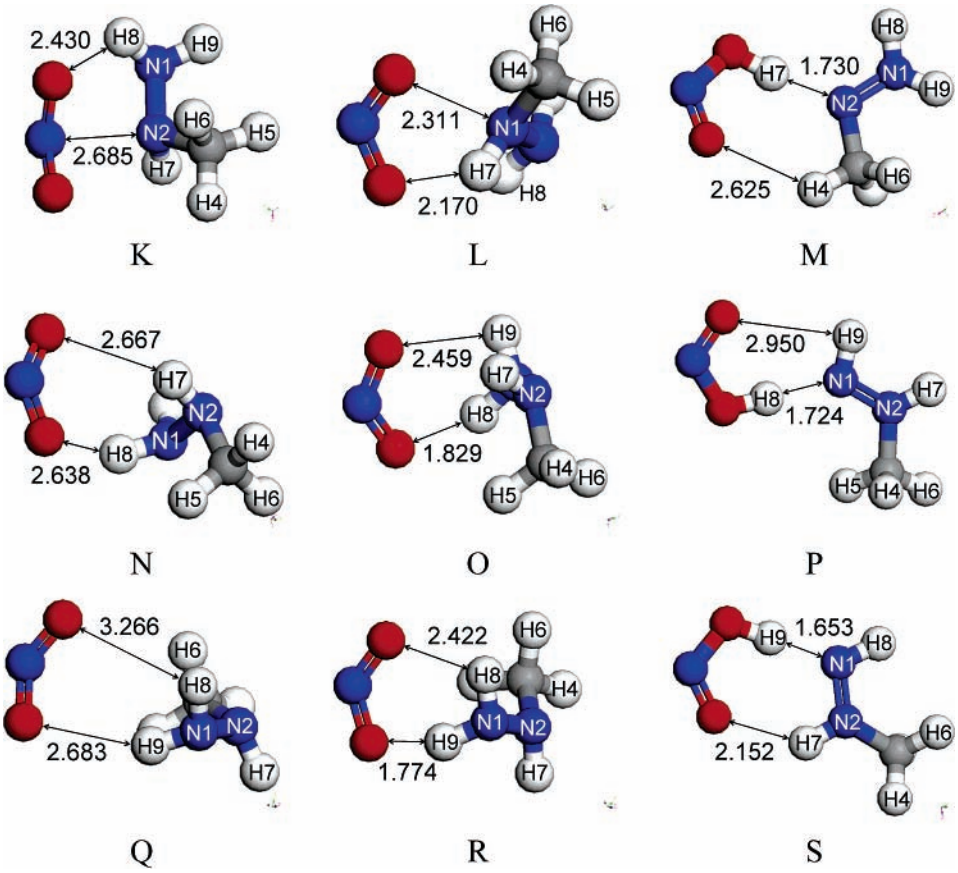


**Figure 3.** Local minima and transition states for the $CH_3NHNH_2 + NO_2$ potential energy surface: configurations K−S. Bond lengths are in angstroms.

**TABLE 5: Relative Zero-Point Corrected Energies[a] (kcal/mol) of Stationary Points for Paths for Reactions 4 and 5**

| species | label | type | method A[b] | method B[c] | method C[d] | method D[e] |
|---|---|---|---|---|---|---|
| $CH_3NHNH_2 + NO_2$ | | RA | 0.0 | 0.0 | 0.0 | 0.0 |
| $CH_3NHNH_2\cdots NO_2$ | [A] | min | −1.7 | −2.7 | −2.7 | −3.2 |
| $CH_3NNH_2\cdots H\cdots NO_2$ | [B] | TS | 11.6 | 12.2 | 8.0 | 14.4 |
| $CH_3NNH_2\cdots HNO_2$ | [C] | min | −2.6 | −3.5 | −5.7 | −4.7 |
| $CH_3NHNH\cdots H\cdots ONO$ | [D] | TS | 4.8 | 3.7 | 0.4 | 3.9 |
| $CH_3NHNH\cdots$*trans*-HONO | [E] | min | −8.5 | −9.0 | −10.7 | −12.2 |
| $CH_3NHNH$(b) + *trans*-HONO | | PA | 2.6 | 2.5 | 2.3 | −1.7 |
| $CH_3NNH_2 + HNO_2$ | | PA | 8.2 | 8.6 | 6.7 | 7.3 |

[a] Energies are relative to the $CH_3NHNH_2$(a)+ $NO_2$ reactant asymptote. Scaled MPWB1K/6-31+G(d,p) ZPVEs have been employed for all methods. [b] CCSD/6-311+G(2df,p)//CCSD/6-31+G(d,p). [c] CCSD(T)/6-311++G(3df,2p)//MPWB1K/6-31+G(d,p). [d] MPWB1K/6-31+G(d,p). [e] CCSD/6-31+G(d,p).

6-31+G(d,p) and (scaled) MPWB1K/6-31+G(d,p) ZPVEs were obtained, the differences in the calculations of the structures' energies relative to the reactant asymptote are less than 0.5 kcal/mol.

## 3. Results and Discussion

**3.1. Reactants and Products.** The MPWB1K/6-31+G(d,p)-optimized geometries of reactant and product structures are displayed in Figure 1, their zero-point corrected energies at the CCSD(T)/6-311++G(3df,2p)//MPWB1K/6-31+G(d,p) and CCSD(T)/6-311+G(2df,p)//CCSD/6-31+G(d,p) levels of theory are provided in Table 1, and selected geometric parameters for each as computed by the MPWB1K/6-31+G(d,p) and CCSD/6-31+G(d,p) models are shown in Table 2. (*Z*-matrix representations for all structures are provided in the Supporting Information.) Two low-energy equilibrium conformers of MMH were observed and characterized. The higher-energy conformer [$CH_3NHNH_2$(b)] is 0.7 kcal/mol above the ground state [$CH_3NHNH_2$(a)], and the lower of the 2 barriers to internal rotation that separates them [$CH_3NHNH_2$(TS1)] is 2.7 kcal/mol above $CH_3NHNH_2$(a)'s level. Only one equilibrium conformer of $CH_3NNH_2$ and two equilibrium conformers of $CH_3NHNH$ [$CH_3NHNH$(a) and $CH_3NHNH$(b)] were observed. $CH_3NHNH$(a) is 2.0 kcal/mol higher in energy than $CH_3NNH_2$, and $CH_3NHNH$(b) is 0.2 kcal/mol higher in energy than $CH_3NHNH$(a). A transition state [$CH_3NHNH$(TS)] corresponding to a barrier to internal rotation separating $CH_3NHNH$(a) and $CH_3NHNH$(b) was also identified. It is 21.0 kcal/mol higher in energy than $CH_3NHNH$(a). $CH_2NHNH_2$ is predicted to be 14.2 kcal/mol higher in energy than $CH_3NNH_2$.

As for the oxygen-containing species, the CCSD(T)/6-311++G(3df,2p)//MPWB1K/6-31+G(d,p) calculations predict that *trans*-HONO is 0.3 kcal/mol lower in energy than *cis*-HONO and 8.1 kcal/mol lower in energy than $HNO_2$. These differences are similar to those predicted by G2-type calculations for structures obtained via MP2/6-311G(d,p) optimizations.[14]

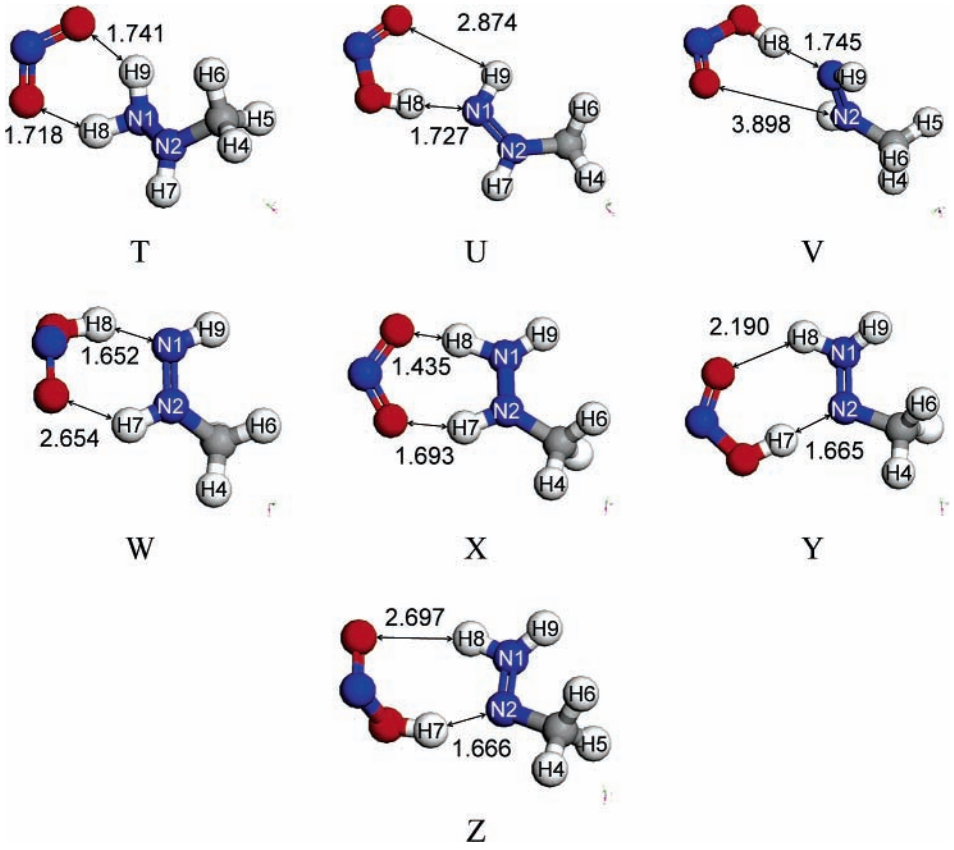


**Figure 4.** Local minima and transition states for the $CH_3NHNH_2 + NO_2$ potential energy surface: configurations T−Z. Bond lengths are in angstroms.

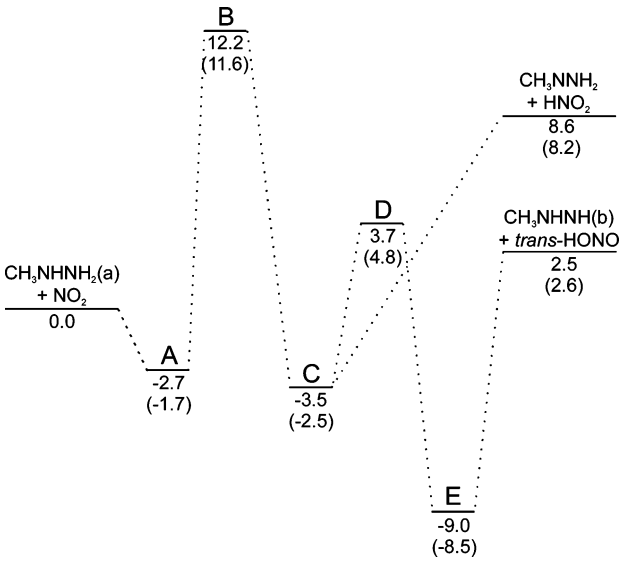


**Figure 5.** Relative energies (in kcal/mol) of stationary points along paths to the $CH_3NNH_2 + HNO_2$ and $CH_3NHNH(b)$+*trans*-HONO product asymptotes. CCSD(T)/6-311++G(3df,2p)//MPWB1K/6-31+G(d,p) and CCSD(T)/6-311+G(2df,p)//CCSD/6-31+G(d,p) results are shown. CCSD(T)/6-311+G(2df,p)//CCSD/6-31+G(d,p) results are in parentheses.

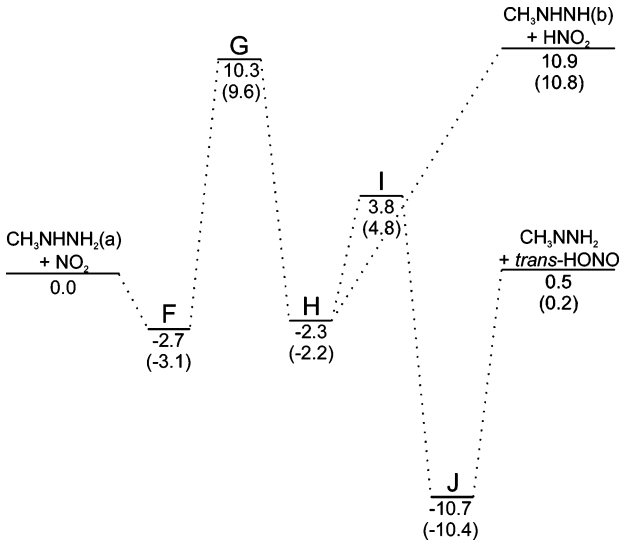


**Figure 6.** Relative energies (in kcal/mol) of stationary points along paths to the $CH_3NHNH(b)+HNO_2$ and $CH_3NNH_2$+*trans*-HONO product asymptotes. CCSD(T)/6-311++G(3df,2p)//MPWB1K/6-31+G(d,p) and CCSD(T)/6-311+G(2df,p)//CCSD/6-31+G(d,p) results are shown. CCSD(T)/6-311+G(2df,p)//CCSD/6-31+G(d,p) results are in parentheses.

A (transition state) barrier to internal rotation separating *cis*-HONO from *trans*-HONO was identified by rotating the H−O−N−O dihedral angle. This transition state, which is referred to in the table as HONO(TS), is predicted to be 10.7 kcal/mol higher in energy than *trans*-HONO.

The MPWB1K/6-31+G(d,p) and CCSD/6-31+G(d,p) optimizations produced reactant and product geometries that were very similar. In the case of bond lengths, all of the MPWB1K/6-31+G(d,p)-determined values (that were measured) are shorter than corresponding CCSD/6-31+G(d,p) values, but all corresponding values are within 0.05 Å of one another. All observed differences between heavy atom−H atom bond lengths determined by the two methods are less than 0.010 Å. And, with two exceptions, observed differences between heavy atom−heavy atom bond lengths fall in the range from 0.020 to 0.035

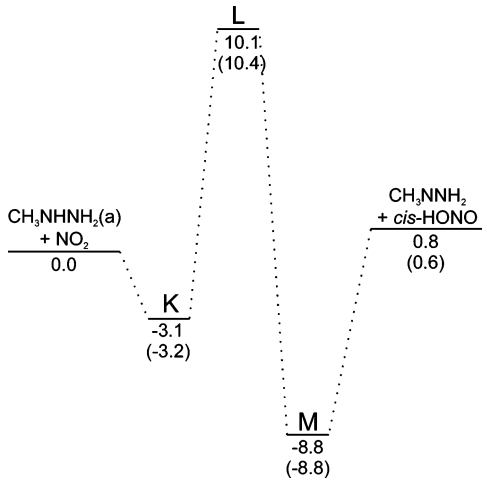


**Figure 7.** Relative energies (in kcal/mol) of stationary points along a path to the $CH_3NNH_2$+*cis*-HONO product asymptote. CCSD(T)/6-311++G(3df,2p)//MPWB1K/6-31+G(d,p) and CCSD(T)/6-311+G-(2df,p)//CCSD/6-31+G(d,p) results are shown. CCSD(T)/6-311+G-(2df,p)//CCSD/6-31+G(d,p) results are in parentheses.

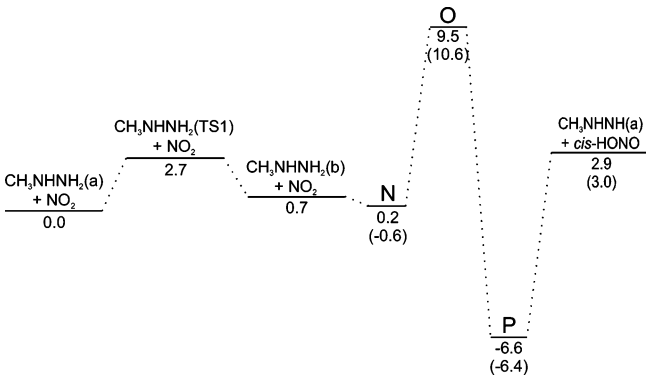


**Figure 8.** Relative energies (in kcal/mol) of stationary points along a path to the $CH_3NHNH(a)$+*cis*-HONO product asymptote. CCSD(T)/6-311++G(3df,2p)//MPWB1K/6-31+G(d,p) and CCSD(T)/6-311+G-(2df,p)//CCSD/6-31+G(d,p) results are shown. CCSD(T)/6-311+G-(2df,p)//CCSD/6-31+G(d,p) results are in parentheses.

Å. The two exceptions are both associated with the longer of the two N−O bonds in *cis*-HONO and *trans*-HONO. In these cases the difference approaches 0.05 Å. For all but one of the simple angles or dihedral angles that were measured, the differences between MPWB1K/6-31+G(d,p) and CCSD/6-31+G(d,p) values are less than 5.0°.

**3.2. Intermediate and Transition State Structures.** Table 3 compares the relative energies of the local minima [min] and transition states [TS] discussed in the sections that follow. Values determined by the CCSD(T)/6-311++(3df,2p)//MPWB1K/6-31+G(d,p) and CCSD(T)/6-311+(2df,p)//CCSD/6-31+G(d,p) models are given with respect to the MMH(a) + $NO_2$ reactant asymptote [RA]. With one exception, it is observed that the differences between the respective values from the two methods are less than 1.2 kcal/mol.

The structure and selected geometric parameters for all of the intermediate and transition state structures given in Table 3 are shown in Figures 2−4. (*Z*-matrix representations for each structure are provided as Supporting Information.) A comparison of selected MPWB1K/6-31+G(d,p)- and CCSD/6-31+G(d,p)-determined bond lengths for transition state structures is provided in Table 4. As found for the reactants and products, the CCSD-calculated bond lengths tend to be slightly longer than corresponding MPWB1K-calculated bond lengths, exceptions being X−H bonds (X = N or O) along the reaction coordinate. In these latter cases, the CCSD-calculated bond lengths are neither consistently longer nor shorter than the MPWB1K-calculated bond lengths, and differences approaching 0.2 Å are observed.

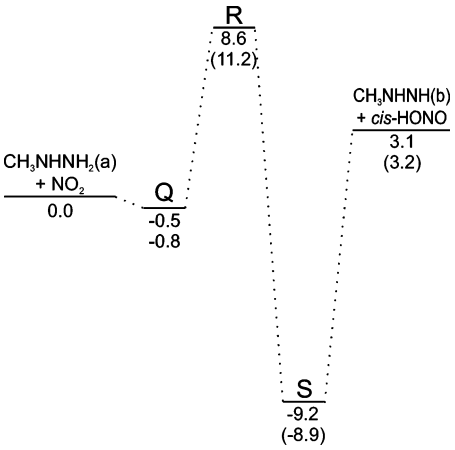


**Figure 9.** Relative energies (in kcal/mol) of stationary points along a path to the $CH_3NHNH(b)$+*cis*-HONO product asymptote. CCSD(T)/6-311++G(3df,2p)//MPWB1K/6-31+G(d,p) and CCSD(T)/6-311+G-(2df,p)//CCSD/6-31+G(d,p) results are shown. CCSD(T)/6-311+G-(2df,p)//CCSD/6-31+G(d,p) results are in parentheses.

**3.3. $CH_3NHNH_2$ + $NO_2$ Reaction Paths.** Paths for reactions 4 and 5 were previously identified and characterized via CCSD/6-31+G(d,p) calculations,[9] and MPWB1K/6-31+G(d,p) calculations were found to produce similar results for them. Figure 5 displays a diagram of energies relative to the reactant asymptote for stationary points of these paths. The paths to the two product asymptotes share a common transition state [B] that connects a $CH_3NHNH_2$−$NO_2$ complex [A] to a $CH_3NNH_2$−$HNO_2$ complex [C]. That transition state is the highest (re: rate-limiting) barrier in both paths. The $CH_3NNH_2$−$HNO_2$ complex connects to a $CH_3NHNH$-*trans*-HONO complex [E] via an H atom exchange reaction. The energy of the transition state for the exchange reaction [D] is 3.7 kcal/mol above the reactant asymptote; i.e., much lower than the energy of the transition state connecting the $CH_3NHNH_2$−$NO_2$ complex to the $CH_3NNH_2$−$HNO_2$ complex.

Table 5 provides a comparison of the relative energies of stationary points for reactions 4 and 5 as computed by the CCSD(T)/6-311++G(3df,2p)//MPWB1K/6-31+G(d,p),MPWB1K/6-31+G(d,p), CCSD(T)/6-311++(2df,p)// CCSD/6-31+G(d,p) and CCSD/6-31+G(d,p) models. Reasonable agreement between the relative energies of most of the equilibrium states is observed, but differences in the relative energies of the transition states are significant. Taken together, the results indicate the need for the refined single point energy calculations.

Like the paths to the $CH_3NNH_2$ + $HNO_2$ and $CH_3NHNH$ + *trans*-HONO product asymptotes, paths to the $CH_3NHNH$ + $HNO_2$ and $CH_3NHNH_2$ + *trans*-HONO product asymptotes; i.e., reactions 2 and 7, were previously identified and (partially) characterized with the CCSD/6-31+G(d,p) model.[9] The search for the $CH_3NHNH\cdots H\cdots NO_2$ transition state at that level of theory was not successful, however, until the structure was found with the MPWB1K/6-31+G(d,p) model and that structure and its force constants employed as a starting point for the CCSD/6-31+G(d,p) optimization. Figure 6 displays a diagram of the relative energies of stationary points of paths for these reactions. Again, the two paths share a common transition state, this time one [G] that connects a $CH_3NHNH_2$−$NO_2$ complex [F] to a $CH_3NHNH$−$HNO_2$ complex [H], and this transition state is the

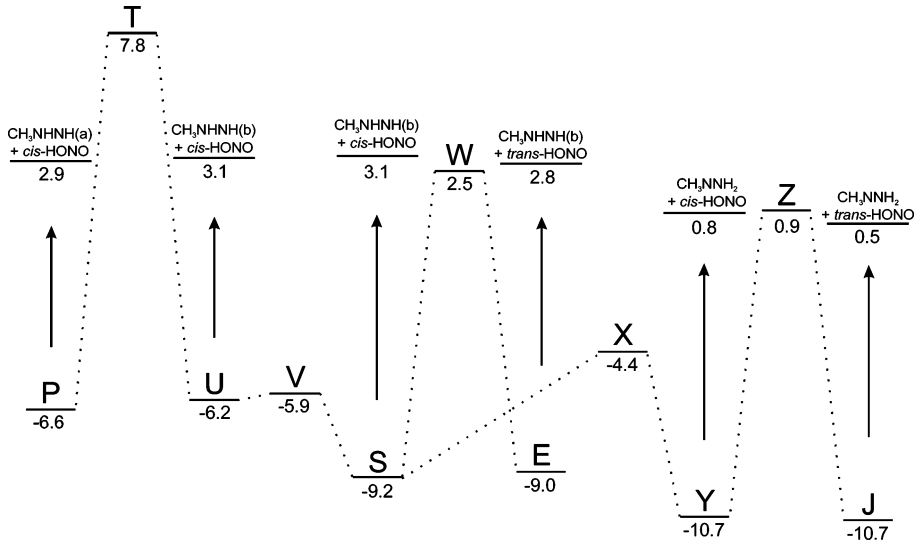


**Figure 10.** Stationary points of paths connecting the product asymptotes. CCSD(T)/6-311++G(3df,2p)//MPWB1K/6-31+G(d,p) results are shown.

highest barrier in both paths. The $CH_3NHNH-HNO_2$ complex connects to a $CH_3NNH_2$−*trans*-HONO complex [J] via an H atom exchange reaction. The transition state for the exchange [I] is (again) much lower in energy than that of the transition state for a one-way transfer.

A somewhat surprising result is the prediction that [G] is lower in energy than [B]. The lower energy of $CH_3NNH_2$ relative to $CH_3NHNH$ indicates that the dissociation energy of the $CH_3N(NH_2)$-H bond is lower than the dissociation energy of the $CH_3NHNH-H$ bond. Coupled with Hammond's postulate,[38] one would expect that [B] would be lower in energy than [G]. The observed result might, however, have been anticipated based on the length of the MMH N−H bond that is broken to form $HNO_2$. In the higher energy case, it is 1.005 Å while in the lower energy case it is 1.013 Å.

Figures 7−9 display diagrams of paths to $CH_3NNH_2$ + *cis*-HONO, $CH_3NHNH$(a) + *cis*-HONO, and $CH_3NHNH$(b) + *cis*-HONO product asymptotes, respectively. Based on Mebel et al.'s results for $NH_3 + NO_2$, it was expected that transition states approximately 7 kcal/mol lower in energy than the $CH_3NNH_2\cdot\cdot\cdot H\cdot\cdot\cdot NO_2$ [B] and $CH_3NHNH\cdot\cdot\cdot H\cdot\cdot\cdot NO_2$ [G] transition states would be found for these paths. Thus, the values observed (8.6−10.1 kcal/mol) are somewhat surprising. Moreover, the low end of the range is found for paths that lead to the formation of $CH_3NHNH$, not $CH_3NNH_2$. The results thus suggest that Catoire et al.'s estimate for the activation energy of reaction 1 (5.9 kcal/mol)[7] is too low.

The lower barriers found for $CH_3NHNH$ production coupled with the possibility that its reaction with $NO_2$ might produce $CH_3NHN$ in addition to $CH_3NNH$ led us to consider whether $CH_3NHNH$ and $CH_3NNH_2$ needed to be distinguished in the chemical kinetics mechanism. Our first approach to examining this issue was to characterize a unimolecular H atom exchange path for $CH_3NHNH$(b) ↔ $CH_3NNH_2$ isomerization. The barrier for the path found was 48.2 kcal/mol, implying isomerization via such a mechanism would not be facile. However, an alternate mechanism is available—namely, an H atom exchange mediated by $NO_2$. Many transition states for such paths had previously been observed,[9] but for the most part they were ignored because their potential relevance to the kinetics of the system was not appreciated.

Figure 10 shows paths which connect various product asymptotes. This manifold may be entered via the minimum energy path from the reactant asymptote, i.e., to [S] from [R]. H atom exchange reactions connect *cis*-HONO-containing complexes with other *cis*-HONO-containing complexes while hindered internal rotations connect *cis*-HONO-containing complexes with *trans*-HONO-containing complexes. In all cases, the energies of these transition states are less than that of the transition state connecting this manifold to the MMH + $NO_2$ reactant asymptote. Therefore, the system can be expected to equilibrate among these product states, thus favoring the formation of $CH_3NNH_2$ and *trans*-HONO. The chemical kinetics mechanism's failure to distinguish between $CH_3NNH_2$ and $CH_3NHNH$ or between *cis*-HONO and *trans*-HONO can therefore be rationalized. However, decomposition paths for $CH_3NHNH$ and the 2 HONOs should be investigated to validate this conclusion.

## 4. Summary

Stationary points of paths for H atom abstraction from $CH_3NHNH_2$ by $NO_2$ have been characterized. The study was greatly facilitated by geometry optimizations performed with MPWB1K/6-31+G(d,p). Five transition states connecting $CH_3NHNH_2-NO_2$ complexes to a manifold that includes $CH_3NHNH-HONO$, $CH_3NNH_2-HONO$, $CH_3NNH_2-HNO_2$, and $CH_3NHNH-HNO_2$ complexes were identified. Two of the transition states connect to $CH_3NNH_2$-containing complexes and three connect to $CH_3NHNH$-containing complexes. The manifold of complexes is, in turn, interconnected through a number of H atom exchange reactions and hindered internal rotations that have relatively low energy barriers. The results suggest that if a generalized step such as reaction 1 is utilized to model the abstraction of an H atom from MMH by $NO_2$, its activation energy should be higher than the (5.9 kcal/mol) value recommended by Catoire et al. The results also provide some justification for neglecting: (1) the production $CH_3NHNH$ and (2) a distinction between *cis*- and *trans*-HONO, in chemical kinetics mechanisms designed for use in modeling MMH/NTO and MMH/IRFNA systems.

**Acknowledgment.** The DoD High Performance Computing Modernization Office supported this project by supplying supercomputer time under the Computing Challenge Project C1A. The computer time was made available at the DoD Major Shared Resources Center at Aeronautical Systems Center, Wright-Patterson Air Force Base, OH.

**Supporting Information Available:** Tables of *Z*-matrix representations of all the structures discussed in this paper including results from both MPWB1K/6-31+G(d,p) and CCSD/6-31+G(d,p) optimizations. This material is available free of charge via the Internet at http://pubs.acs.org.

## References and Notes

(1) Schmidt, E. W. *Hydrazine and Its Derivatives: Preparation, Properties, Applications*; Wiley: New York, 2001.

(2) Nusca, M. J.; Michaels, R. S. *39th AIAA/ASME/SAE/ASEE Joint Propulsion Conference*; 2003; American Institute of Aeronautics and Astronautics (AIAA): Reston, Virginia, 2003.

(3) Nusca, M. J.; Michaels, R. S. *40th AIAA/ASME/SAE/ASEE Joint Propulsion Conference*; 2004; American Institute of Aeronautics and Astronautics (AIAA): Reston, Virginia, 2004.

(4) Vanderhoff, J. A.; Anderson, W. R.; Kotlar, A. J. In *Proceedings of the 29th JANNAF Combustion Subcommittee Meeting*; CPIA Publication 593; Chemical Propulsion Information Agency (CPIA): Columbia, Maryland, 1992; Vol. II, p 225. Anderson, W. R.; Ilincic, N. Meagher, N. E.; Seshadri, K.; Vanderhoff, J. A. *Proceedings of the 32nd JANNAF Combustion Subcommittee Meeting and 1995 Propulsion Systems Hazards Subcommittee Meeting*; CPIA Publication 638; Chemical Propulsion Information Agency (CPIA): Columbia, Maryland, 1995; Vol. I, p 197.

(5) Smith, G. P.; Golden, D. M.; Frenklach, M.; Moriarty, N. W.; Eiteneer, B.; Goldenberg, M.; Bowman, C. T.; Hanson, R. K.; Song, S.; Gardiner, W. C.; Lissianski, V. V. Qin Z. http://www.me.berkeley.edu/gri_mech/.

(6) Catoire, L.; Ludwig, T.; Bassin, X.; Dupre, G.; Palliard, C. *Proceedings of the 27th Symposium (International) on Combustion*; The Combustion Institute: Pittsburgh, 1998; pp 2359−2365.

(7) Catoire, L.; Chaumeix, N.; Paillard, C. *J. Prop. Power* **2004**, *20*, 87.

(8) Catoire, L.; Swihart, M. T. *J. Prop. Power* **2002**, *18*, 1242.

(9) McQuaid, M. J.; Anderson, W. R.; Kotlar, A. J.; Nusca, M. J.; Ishikawa, Y. *Proceedings of the Sixth International Symposium on Special Topics in Chemical Propulsion*; Kuo, K., Ed. 2005.

(10) Kee, R. J.; Rupley, F. M.; Miller, J. A. Sandia Report SAND89-8009; 1989.

(11) Sawyer, R. F.; Glassman, I. *Proceedings of the 11*th Symposium *(International) on Combustion* 1967; The Combustion Institute: Pittsburgh, pp 861−869.

(12) Tuazon, E. C.; Carter, W. P. L.; Brown, R. V.; Winer, A. M.; Pitts, J. N. *J. Phys. Chem.* **1983**, *87*, 1600.

(13) Durgapal, U. C.; Venugopal, V. K. *AIAA J.* **1974**, 1611−1612.

(14) Mebel, A. M.; Diau, E. W. G.; Lin, M. C.; Morokuma, K. *J. Phys. Chem.* **1996**, *100*, 7517.

(15) Zhao, Y.; Truhlar, D. G. *J. Phys. Chem. A* **2004**, *108*, 6908.

(16) Peterson, G. A.; Al-Laham, M. A. *J. Chem. Phys.* **1991**, *94*, 6018.

(17) Peterson, G. A.; Bennett, A.; Tensfeldt, T. G.; Al-Laham, M. A.; Shirley, W. A.; Mantzaris, J. *J. Chem. Phys.* **1988**, *89*, 2193.

(18) Clark, T.; Chandrashakar, J.; Spitznagel, G. W.; Schleyer, P. V. R. *J. Comput. Chem.*, **1983**, *4*, 294.

(19) Cizek, J. *Adv. Chem. Phys.* **1969**, *14*, 35.

(20) Purvis, G. D.; Bartlett, R. J. *J. Chem. Phys.* **1982**, *76*, 1910.

(21) Scuseria, G. E.; Janssen, C. L.; Schaefer, H. F. *J. Chem. Phys.* **1988**, *89*, 7382.

(22) Scuseria, G. E.; Schaefer, H. F. *J. Chem. Phys.* **1989**, *90*, 3700.

(23) Pople, J. A.; Head-Gordon, M.; Raghavachari, K. *J. Chem. Phys.* **1987**, *87*, 5968.

(24) Hehre, W. J.; Radom, L.; Schleyer, P. v. R. *Ab Initio Molecular Orbital Theory*; Wiley: New York, 1986.

(25) Lee, C.; Yang, W.; Parr, R. G. *Phys. Rev. B* **1988**, *37*, 785.

(26) Miehlich, B.; Savin, A.; Stoll, H.; Preuss, H. *Chem. Phys. Lett.* **1989**, *157*, 200.

(27) Becke, A. D. *J. Chem. Phys.* **1993**, *98*, 5648.

(28) Krishnan, R.; Binkley, J. S.; Seeger, R.; Pople, J. A. *J. Chem. Phys.* **1980**, *72*, 650.

(29) Lynch, B.J.; Fast, P. L.; Harris, M.; Truhlar, D. G. *J. Phys. Chem. A* **2000,** *104*, 4811.

(30) Head-Gordon, M.; Pople, J. A.; Frisch, M. J. *Chem. Phys. Lett.* **1988**, *153*, 503.

(31) Frisch, M. J.; Head-Gordon, M.; Pople, J. A. *Chem. Phys. Lett.* **1990**, *166*, 275.

(32) Frisch, M. J.; Head-Gordon, M.; Pople, J. A. *Chem. Phys. Lett.* **1990**, ***166***, 281.

(33) Head-Gordon, M.; Head-Gordon, T. *Chem. Phys. Lett.* **1994**, *220*, 122.

(34) Saebo, S.; Almlof, J. *Chem. Phys. Lett.* **1989**, *154*, 83.

(35) Gonzalez, C.; Schlegel, H. B. *J. Chem. Phys.* **1989**, *90*, 2154.

(36) Gonzalez, C.; Schlegel, H. B. *J. Phys. Chem.* **1990**, *94*, 5523.

(37) Frisch, M. J.; Trucks, G. W.; Schlegel, H. B.; Scuseria, G. E.; Robb, M. A.; Cheeseman, J. R.; Montgomery, J. A., Jr.; Vreven, T.; Kudin, K. N.; Burant, J. C.; Millam, J. M.; Iyengar, S. S.; Tomasi, J.; Barone, V.; Mennucci, B.; Cossi, M.; Scalmani, G.; Rega, N.; Petersson, G. A.; Nakatsuji, H.; Hada, M.; Ehara, M.; Toyota, K.; Fukuda, R.; Hasegawa, J.; Ishida, M.; Nakajima, T.; Honda, Y.; Kitao, O.; Nakai, H.; Klene, M.; Li, X.; Knox, J. E.; Hratchian, H. P.; Cross, J. B.; Bakken, V.; Adamo, C.; Jaramillo, J.; Gomperts, R.; Stratmann, R. E.; Yazyev, O.; Austin, A. J.; Cammi, R.; Pomelli, C.; Ochterski, J. W.; Ayala, P. Y.; Morokuma, K.; Voth, G. A.; Salvador, P.; Dannenberg, J. J.; Zakrzewski, V. G.; Dapprich, S.; Daniels, A. D.; Strain, M. C.; Farkas, O.; Malick, D. K.; Rabuck, A. D.; Raghavachari, K.; Foresman, J. B.; Ortiz, J. V.; Cui, Q.; Baboul, A. G.; Clifford, S.; Cioslowski, J.; Stefanov, B. B.; Liu, G.; Liashenko, A.; Piskorz, P.; Komaromi, I.; Martin, R. L.; Fox, D. J.; Keith, T.; Al-Laham, M. A.; Peng, C. Y.; Nanayakkara, A.; Challacombe, M.; Gill, P. M. W.; Johnson, B.; Chen, W.; Wong, M. W.; Gonzalez, C.; Pople, J. A. Gaussian, Inc.: Wallingford CT, 2004.

(38) Hammond,G. S. *J. Am. Chem. Soc.* **1955**, *77*, 334.